RSC Advances

PAPER

View Article Online
View Journal | View Issue

Cite this: *RSC Adv.*, 2017, **7**, 27405

Enhanced activity of $CuO/K_2CO_3/MgAl_2O_4$ catalyst for lean NO_x storage and reduction at high temperatures†

Yaoyao Liu,[a] Lihong Guo,[ab] Dongyue Zhao,[a] Xingang Li,*[a] Zhongnan Gao,[a] Tong Ding,*[a] Ye Tian[a] and Zheng Jiang[c]

Herein, we designed a new NO_x storage and reduction $CuO/K_2CO_3/MgAl_2O_4$ catalyst operating within the high temperature region of 350–550 °C. Compared with the Al_2O_3 supported catalyst with the same Cu and K loading, it exhibits superior NO_x storage and reduction performance. The NO_x reduction percentage (NRP) of the $CuO/K_2CO_3/MgAl_2O_4$ catalyst remains above 90% over a wide temperature range (400–550 °C), and reaches the highest NRP of 99.9% at 450 °C with the N_2 selectivity of 99.7%. Uncovered CuO particles with better reducibility exist on the $CuO/K_2CO_3/MgAl_2O_4$ catalyst, with the high NO_x oxidation and reduction ability above 400 °C. Potassium carbonates on the $CuO/K_2CO_3/MgAl_2O_4$ catalyst mainly exist in three forms, including free ionic carbonate, bridging bidentate carbonate and chelating bidentate carbonate. Under lean-burn conditions, most of carbonates on the $CuO/K_2CO_3/MgAl_2O_4$ catalyst can store NO_x to form nitrates, but only parts of them participate in NO_x storage on the $CuO/K_2CO_3/Al_2O_3$ catalyst. The $MgAl_2O_4$ support offers additional sites for NO_x adsorption, while the formed nitrate on it shows low thermal stability. So, NO_x is mainly stored on K_2CO_3 at high temperatures, because $MgAl_2O_4$ can enhance the thermal stability of the supported K_2CO_3 on it. Our results show that the thermal stability of K_2CO_3 directly determines the thermal stability of the formed nitrates. Accordingly, the $CuO/K_2CO_3/MgAl_2O_4$ catalyst shows the high NSR activity because of the efficient redox ability of CuO and high thermal stability of K_2CO_3 at high operating temperatures.

Received 18th March 2017
Accepted 16th May 2017

DOI: 10.1039/c7ra03200e

rsc.li/rsc-advances

1. Introduction

Modern lean-burn engines usually operate at a high air/fuel ratio, which results in a high fuel utilization efficiency.[1] Unfortunately, the emitted NO_x (NO and NO_2) is hardly removed over the conventional three way catalysts (TWC) because of the presence of excess oxygen. With the increasing NO_x emission limit, it is urgent to develop effective catalytic after-treatment systems.[2,3] To solve this problem, methodologies for NO_x storage and reduction (NSR) and selective catalytic reduction (SCR) of NO_x are being developed.[4,5] Presently, the NSR technology is a preferred choice especially for light duty lean-burn engines.[6,7]

The process of NSR, also known as lean NO_x trap (LNT), is operated in alternative lean-burn/fuel-rich atmospheres, which mainly includes: NO_x is captured by alkali/alkali earth components (*e.g.* barium and potassium) within a long lean-burn period (1–2 min); the trapped NO_x species is released and then reduced to harmless N_2 by precious group metals (*e.g.* Pt and Rh) within a subsequent short fuel-rich period (3–20 s).[4,8] High NO_x removal efficiency has been achieved over the $Pt/BaO/Al_2O_3$ catalyst developed by the Toyota company within a narrow temperature window of 300–400 °C.[9–15] However, some newly developed lean-burn gasoline engine technologies, such as gasoline direct injection (GDI), are required to operate at higher temperatures than normal. Under this condition, the activity of the traditional $Pt/BaO/Al_2O_3$ NSR catalyst significantly drops.[16,17] When the operating temperature exceeds 400 °C, the solid-phase reaction between BaO and Al_2O_3 to form $BaAl_2O_4$ will lower the surface area and reduce the NO_x storage sites.[18] Pt sintering also hampers the reduction of NO_x from cycle to cycle.[19,20] Furthermore, the low thermal stability of barium nitrates declines its application at high operating temperatures, which is believed to be the essential factor to limit the NO_x storage capacity.[18,21] Thus, it is urgent to develop a NSR catalyst with good high-temperature performance.

[a]*Collaborative Innovation Center of Chemical Science and Engineering (Tianjin), Tianjin Key Laboratory of Applied Catalysis Science and Engineering, School of Chemical Engineering & Technology, Tianjin University, Tianjin 300072, P. R. China. E-mail: xingang_li@tju.edu.cn*

[b]*School of Chemistry and Chemical Engineering, Henan University of Technology, Zhengzhou 450001, P. R. China*

[c]*Shanghai Synchrotron Radiation Facility, Shanghai Institute of Applied Physics, Chinese Academy of Sciences, Shanghai, 201800, P. R. China*

† Electronic supplementary information (ESI) available. See DOI: 10.1039/c7ra03200e

It was reported that mixing an alkaline earth metal oxide with Al_2O_3 could enhance the basicity of the support and also improve the thermal stability of the trapped nitrates.[16] $MgAl_2O_4$, as one of these mixed oxides, has been employed as support of high-temperature NSR catalysts. Through supported on $MgAl_2O_4$, the stability of nitrate species is strongly improved whether on potassium sites or barium sites,[16,18] and Pt sintering can also be effectively inhibited.[17] Additionally, the $MgAl_2O_4$ support can provide extra storage sites for NO_x.[22] Hence, we chose $MgAl_2O_4$ as the support of NSR catalysts operated at high temperatures.

Additionally, to lower the price of NSR catalysts, it is valuable to substitute Pt with non-noble metal components. In the previous study, the perovskite-type oxides were used in replacement of platinum-based catalyst, such as $BaFeO_{3-x}$, $LaCoO_3$ and $La_{1-x}Sr_xCoO_3$.[23–28] The transition metal elements of manganese and copper were also studied as substitutes for platinum.[29,30] It was reported that $Cu/K_2Ti_2O_5$ could be applied over a wide temperature range (200–600 °C) with the mutual transformation of different structures.[31]

As for the storage material, it is generally admitted that potassium-based catalysts have higher ability to storage NO_x at high temperatures (above 400 °C) than barium-based ones due to its stronger basicity and better mobility.[32] Potassium is more suitable as the storage element for the high-temperature NSR catalyst.[17]

Based on the above analysis, it is interesting to design a new NSR catalyst with CuO as the NO_x oxidation and reduction center, potassium as the NO_x storage element and $MgAl_2O_4$ as the support material. To the best of our knowledge, the reasonably designed $CuO/K_2CO_3/MgAl_2O_4$ catalyst herein has not been reported before.

In this study, we prepared the $CuO/K_2CO_3/MgAl_2O_4$ catalyst by successive impregnation method. The Al_2O_3-supported catalyst with the same Cu and K loading was also prepared for comparison. The NO_x storage/reduction performance within 350–550 °C of the two catalysts was comparatively investigated. Then, we characterized the catalysts by the X-ray diffraction (XRD), X-ray absorption near-edge structures (XANES), X-ray photoelectron spectroscopy (XPS), scanning electron microscopy (SEM), Fourier-transforming infrared spectra (FT-IR), H_2 temperature-programmed reduction (H_2-TPR), temperature-programmed desorption of CO_2 (CO_2-TPD) and temperature-programmed desorption of NO_x (NO_x-TPD). Through the results of the above characterizations, we investigated the states of K- and Cu-species in $CuO/K_2CO_3/MgAl_2O_4$ and $CuO/K_2CO_3/Al_2O_3$ catalysts. We also discussed the thermal stability of nitrate on the catalysts and revealed how the $CuO/K_2CO_3/MgAl_2O_4$ catalyst improved the NSR performance at high temperatures.

2. Experimental section

2.1. Support and catalyst preparation

2.1.1. Support preparation. The $MgAl_2O_4$ support was prepared by co-precipitation method. A certain amount of $Mg(NO_3)_2 \cdot 6H_2O$ and $Al(NO_3)_3 \cdot 9H_2O$ was dissolved and mixed with vigorous stirring. The pH value of the aqueous solution was adjusted to 9.5 by addition of $NH_3 \cdot H_2O$. The mixture was aged at 65 °C for 12 h and then filtrated. The obtained solid was dried at 120 °C for 12 h and then calcined at 800 °C for 5 h. The commercial γ-Al_2O_3 support (Tianjin Chemical Research & Design Institute) was pre-treated at 600 °C before using.

2.1.2. Catalyst preparation. The $CuO/K_2CO_3/MgAl_2O_4$ catalyst was prepared by successive incipient wetness impregnation. The support was immersed into the solution of $Cu(NO_3)_2 \cdot 3H_2O$, dried at 120 °C and then calcined at 600 °C for 4 h. Subsequently, K_2CO_3 was loaded on the above powder by incipient wetness impregnation. The final sample was obtained after calcination at 600 °C for 2 h. The weight loadings of Cu and K were both 10%.

For comparison, the $CuO/K_2CO_3/Al_2O_3$ catalyst was also prepared by incipient wetness impregnation with the same process. The weight loadings of Cu and K were both 10%. The $K_2CO_3/MgAl_2O_4$, K_2CO_3/Al_2O_3, $CuO/MgAl_2O_4$ and CuO/Al_2O_3 samples were prepared with the same method. The weight loadings of Cu or K was also 10%.

2.2. Catalyst characterization

The measurement of the specific surface area (S_{BET}) was carried out at −196 °C on a Quantachrome QuadraSorb SI instrument. Before measurements, the samples were degassed in vacuum at 300 °C for 3 h to remove the adsorbed species.

XRD analysis was conducted on an X'pert Pro rotatory diffractometer (PANAlytical Company, Cu Kα radiation λ = 0.15418 nm) operating at 40 mA and 40 kV. The diffraction data were collected in the 10 to 90° range at a step size of 0.02°. The crystallite sizes of CuO were calculated by using Scherrer equation:

$$D = \frac{K\lambda}{\beta \cos \theta}$$

D is the crystallite size. K is a constant. λ is the wavelength of the X-ray device. β is the full weight half maximum. θ is the Bragg's angle.

XPS measurements were carried out by using a PHI-1600 ESCA spectrometer with Mg Kα (1253.6 eV) as radiation source. The base pressure in sample chamber was 5×10^{-8} Pa. The binding energy (BE) peak of C 1s at 284.6 eV was employed to be standard to calibrate the recorded spectra.

The tests of XANES were performed on the 14 W1 beamline of shanghai Synchrotron Radiation Facility. Tests were operated at 250 mA and 3.5 GeV. A Si (1 1 1) double-crystal monochromator was employed to monochromatize X-ray. A copper foil was used for energy calibration.

The morphologies of the catalysts were observed by SEM (S-4800, Hitachi). Before the SEM test, the samples were coated on a thin Pt layer to improve the electrical conductivity.

H_2-TPR experiments were carried out on the TP-5079 TPDRO apparatus (Xian quan). The reduction gas is 8 vol% H_2/N_2 with a flow rate of 30 mL min^{-1}. The weight of sample used for test is 30 mg. The sample was heated from room temperature (RT) to 900 °C, and the heating rate is 10 °C min^{-1}.

CO_2-TPD experiments derived from carbonate decomposition were carried out on a Thermo-Finnigan TPDRO 1100. The samples were heated in highly pure helium gas (20 mL min^{-1}) from RT to 900 °C. The heating rate was 10 °C min^{-1}.

NO_x-TPD test was conducted in a quartz-tubular continuous flow reactor (i.d. = 4 mm). The samples were heated in pure N_2 (400 mL min^{-1}) from 50 °C to 750 °C and the temperature ramp is 5 °C min^{-1}. Before the measurements, the samples were saturated with NO_x in the lean gas (400 ppm of NO, 5% O_2, balanced by N_2) at 450 °C.

The Fourier-transforming infrared spectroscopy (FT-IR) experiment was performed on a Thermo Nicolet Nexus spectrometer. The fresh sample and KBr were mixed with a weight ratio of 1 : 100, and pressed into a pellet. The spectra based on 32 scans were collected in 400–4000 cm^{-1} with resolution of 4 cm^{-1}. The spectra were recorded in air at RT.

2.3. Activity tests

The isothermal NO_x storage and reduction experiments of catalysts were carried out in a quartz-tubular continuous flow reactor (i.d. = 4 mm) using 240 mg of the fresh catalysts (40–60 mesh) from 350 to 550 °C with an increment of 50 °C. It was measured by 20 lean/rich (L/R) cycles (L/R = 50/10 s; lean gas 400 ppm of NO, 5% O_2, balanced by N_2; rich gas 1000 ppm C_3H_6, balanced by N_2). The NO_x concentrations were monitored online by a chemiluminescence NO–NO_2–NO_x analyzer (Model 42i-HL, Thermo Scientific). The total gas flow rate was 400 mL min^{-1}, corresponding to a weight hourly space velocity of 100 000 mL g^{-1} h^{-1}. Meanwhile, the concentration of the byproduct N_2O was monitored online by a N_2O modular gas analyzer (S710, SICK MAIHAK).

The isothermal NO_x storage experiments of the catalysts were carried out in the lean atmosphere (400 ppm of NO, 5% O_2, balanced by N_2) in the same reactor as above mentioned. The NO_x concentrations were also monitored by the same analyzer. The total gas flow rate was 400 mL min^{-1}, corresponding to a weight hourly space velocity of 100 000 mL g^{-1} h^{-1}.

The NO_x reduction percentage (NRP) was calculated according to the steady lean/rich cycle as the following formula:

$$\mathrm{NPR} = \frac{[\mathrm{NO}_x]_{\mathrm{inlet}} \times t_1 - \int [\mathrm{NO}_x]_{\mathrm{outlet}} \mathrm{d}t}{[\mathrm{NO}_x]_{\mathrm{inlet}} \times t_1} \times 100\%$$

The NSC was taken after the NO_x storage process prolonged 60 min and calculated as the following formula:

$$\mathrm{NSC} = \frac{[\mathrm{NO}_x]_{\mathrm{inlet}} \times V \times t_2}{N_0 \times m} \times \text{storage ratio} \times 10^{-6}\ \text{mmol g}^{-1}$$

The storage ratio was calculated as the following formula:

$$\text{Storage ratio} = \frac{[\mathrm{NO}_x]_{\mathrm{inlet}} \times t_2 - \int [\mathrm{NO}_x]_{\mathrm{outlet}} \mathrm{d}t}{[\mathrm{NO}_x]_{\mathrm{inlet}} \times t_2}$$

$[NO_x]$ and $[NO_2]$ is the concentration of NO_x and NO_2 in ppm unit, inlet and outlet refer to the inlet gas and the out gas, respectively. V is the flow rate of the inlet gas, N_0 is 22.4 L mol^{-1}, m is the weight of the sample, t_1 is the lean period in one L/R cycle, t_2 is 60 min, storage radio is the percentage of the stored NO_x to the introduced one.[33]

3. Results and discussion

3.1. NO_x storage capacity measurement

NO_x storage tests were carried out in the temperature range of 350–550 °C. The evolution of outlet NO_x is depicted in Fig. 1. The NSC was calculated and summarized in Table 1. Fig. 1a shows the NSC profiles of the $CuO/K_2CO_3/MgAl_2O_4$ catalyst at the different temperatures. The NO_x storage capacity of the $CuO/K_2CO_3/MgAl_2O_4$ catalyst varies with the increased reaction temperature. At 350 °C, the NO_x trapping kinetics is too slow, inducing the low NSC. Fig. 1a shows that after introducing the feeding gas above 400 °C, a rapid NO_x storage behavior occurs and the NO_x signal diminishes sharply. Subsequently, the "lean trap" period is observed, namely the stage during which NO_x is completely captured on the catalysts and no NO_x is released. Then, the NO_x concentration gradually recovers to the inlet level until saturation. Probably, CuO is activated above 400 °C for NO oxidation to generate NO_2, which is beneficial to NO_x storage under lean-burn conditions.[34,35] Meanwhile, the stored NO_x gets thermally unstable. With the rising of the reaction temperature, the desorption rate of the released NO_x from the catalysts is accelerated, as well as the equilibrium of the NO_x storage process. The largest NSC uptake of the $CuO/K_2CO_3/MgAl_2O_4$ catalyst is obtained at 450 °C, which is the optimum

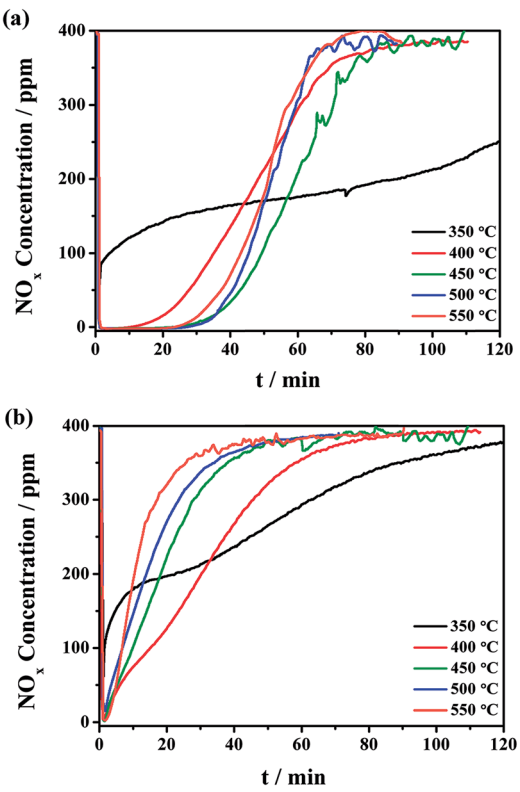

Fig. 1 Isothermal NO_x storage curves of the (a) $CuO/K_2CO_3/MgAl_2O_4$ and (b) $CuO/K_2CO_3/Al_2O_3$ catalysts at the different temperatures.

Table 1 NRP, NSC and NO to NO_2 conversion of the catalysts

Catalysts	T (°C)	NRP (%)	NSC (mmol g^{-1})	NO to NO_2 conversion (%)
$CuO/K_2CO_3/MgAl_2O_4$	350	75.6	1.09	24.1
	400	97.7	1.31	32.8
	450	99.9	1.56	34.0
	500	99.0	1.48	24.3
	550	94.7	1.42	19.6
$CuO/K_2CO_3/Al_2O_3$	350	23.6	0.80	14.1
	400	80.8	0.88	33.3
	450	78.6	0.57	32.7
	500	71.6	0.49	23.8
	550	37.5	0.38	18.9

temperature for the NO_x storage reaction. The "lean trap" period lasts for more than 20 min and the NSC value is 1.56 mmol g^{-1} at 450 °C, which is comparable to or even better than the literature data.[17,36] When the reaction temperature continues to increase, the NSC of the $CuO/K_2CO_3/MgAl_2O_4$ catalyst decreases slightly because a small amount of the trapped NO_x decomposes at high temperatures. Fig. 1b shows the NO_x concentration profiles on the $CuO/K_2CO_3/Al_2O_3$ catalyst at the different temperatures. Similarly, the $CuO/K_2CO_3/Al_2O_3$ catalyst also presents a volcano-type tendency of NSC values in the temperature range of 350–550 °C. Maximum storage capacity is achieved at 400 °C on $CuO/K_2CO_3/Al_2O_3$ and the NSC value is 0.88 mmol g^{-1}.

Differently from the $CuO/K_2CO_3/MgAl_2O_4$ catalyst, the $CuO/K_2CO_3/Al_2O_3$ catalyst nearly presents no "lean trap" period in the NO_x storage profiles. Additionally, the $CuO/K_2CO_3/MgAl_2O_4$ catalyst achieves maximum NSC value at 450 °C, which is 50 °C higher than that of the $CuO/K_2CO_3/Al_2O_3$ catalyst. With further increasing the reaction temperature above 400 °C, the NSC value of the $CuO/K_2CO_3/Al_2O_3$ catalyst decreases seriously, whereas, the $CuO/K_2CO_3/MgAl_2O_4$ catalyst can maintain the large NSC values, making it suitable for the NSR reaction at high temperatures. The NO to NO_2 conversion of the $CuO/K_2CO_3/MgAl_2O_4$ and $CuO/K_2CO_3/Al_2O_3$ catalysts was also measured, and the results were calculated and summarized in Table 1. The NO to NO_2 conversions of the two catalysts are very similar because the oxidation of NO to NO_2 is thermodynamically limited at high temperatures.[5,37,38]

The distinct difference of the NO_x storage behavior at high temperature between the $CuO/K_2CO_3/MgAl_2O_4$ and $CuO/K_2CO_3/Al_2O_3$ catalysts probably results from the different thermal stability of the formed nitrate during the NO_x storage reaction. To investigate the thermal stability of the trapped NO_x on the catalysts, the NO_x-TPD experiments were conducted after the saturated adsorption of NO_x at 450 °C. Fig. 2 shows the NO_x-TPD profiles of the $CuO/K_2CO_3/MgAl_2O_4$, $CuO/K_2CO_3/Al_2O_3$ and $CuO/MgAl_2O_4$ catalysts. In the profile of the $CuO/MgAl_2O_4$, a single NO_x desorption peak is observed at 365 °C, which is attributed to the decomposition of nitrates species formed on the $MgAl_2O_4$ support, confirming that the support offers additional sites for NO_x adsorption. It is likely caused by the strong basicity of $MgAl_2O_4$. However, the $MgAl_2O_4$ support is not the main NO_x storage sites at the high temperatures as indicated by its small desorption amount and poor thermal stability. The desorption peak located at 481 °C in the profile of the $CuO/K_2CO_3/Al_2O_3$ catalyst can be ascribed to the decomposition of KNO_3 on it. Two desorption peaks are clearly observed in the profile of the $CuO/K_2CO_3/MgAl_2O_4$ catalyst. The first peak at 365 °C is assigned to the NO_x desorption from the $MgAl_2O_4$ support as mentioned above. The latter peak appearing at 649 °C can be attributed to the desorption of the stored NO_x species on K_2CO_3. Thus, the K_2CO_3 is identified as the main NO_x storage sites according to the large desorption amount and high thermal stability. Meanwhile, a distinct difference in the decomposition temperatures of KNO_3 between the $CuO/K_2CO_3/Al_2O_3$ (481 °C) and $CuO/K_2CO_3/MgAl_2O_4$ catalysts (649 °C) is observed, suggesting the higher thermal stability of the nitrates on the K sites of the $CuO/K_2CO_3/MgAl_2O_4$ catalyst, which is the main reason of its higher NO_x storage ability at high temperatures.

The components of CuO and K_2CO_3 in the catalyst are designed to act as the NO_x oxidation sites and storage sites, respectively. To clarify the roles of these two components, the stationary NO_x storage tests were also performed over the K_2CO_3-free or CuO-free catalysts. In Fig. S1,† the K_2CO_3-free catalyst of $CuO/MgAl_2O_4$ and CuO-free catalysts of K_2CO_3/Al_2O_3 and $K_2CO_3/MgAl_2O_4$ show the poor NO_x adsorbability. The NSC of the $CuO/MgAl_2O_4$ sample is only 0.11 mmol g^{-1}, because of the absence of K_2CO_3, suggesting that K_2CO_3 is the main NO_x storage sites. The NSC values of the K_2CO_3/Al_2O_3 and $K_2CO_3/MgAl_2O_4$ catalysts are 0.43 mmol g^{-1} and 0.60 mmol g^{-1}, respectively. The decline in the NSC values suggests that the NO oxidation ability of CuO plays a significant role in the NO_x storage process, because NO_2 oxidized from NO is considered to be more easily captured than NO over NSR catalysts.[4,8,39] The result above indicates that both the CuO and K_2CO_3 play the important roles in the NO_x storage process.

3.2. NO_x storage/reduction in the lean–rich cycles

The NO_x storage and reduction tests in the periodical lean/rich cyclic atmospheres (50 s/10 s) were carried out in the temperature range of 350–550 °C. The evolution of outlet NO_x is depicted

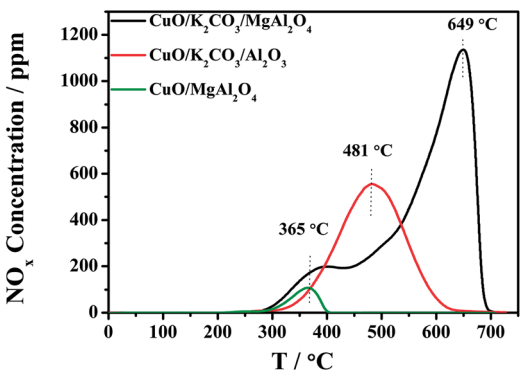

Fig. 2 NO_x-TPD profiles of the catalysts.

in Fig. 3. The NRP was calculated and summarized in Table 1. Fig. 3a shows the concentration of outlet NO_x for the CuO/K_2CO_3/$MgAl_2O_4$ catalyst during the lean–rich cycles. The NSR performance of the CuO/K_2CO_3/$MgAl_2O_4$ catalyst behaves differently depending on the reaction temperatures. At 350 °C, the NRP of the catalyst is 75.6%. The escaping NO_x increases with the prolonged operating period because the NO_x can hardly be reduced. When the reaction temperature is above 400 °C, the NSR performance of the CuO/K_2CO_3/$MgAl_2O_4$ catalyst improves greatly. As the profiles of the NO_x concentration during the lean–rich cycles at 400–550 °C show, NO_x in the feeding gas is captured completely in the lean period firstly; once switched to the rich period, the outlet NO_x concentration is quite low, suggesting that most of the NO_x can be reduced and nearly no NO_x escapes. At 450 °C, the highest NRP of 99.9% is achieved. As the temperature continues to rise, the NRP deceases slightly. The NRP of CuO/K_2CO_3/$MgAl_2O_4$ catalyst can remain above 90% over a wide temperature range (400–550 °C). During the 20 lean–rich cycles, little N_2O is produced as byproduct (Fig. S2†). The selectivity of 99.7% is obtained on the CuO/K_2CO_3/$MgAl_2O_4$ catalyst at 450 °C. Fig. 3b shows the concentration of outlet NO_x for the CuO/K_2CO_3/Al_2O_3 catalyst during the lean–rich cycles. The NO_x reduction ability of the CuO/K_2CO_3/Al_2O_3 catalyst at 350 °C is only 23.6%. At 400 °C, the CuO/K_2CO_3/Al_2O_3 catalyst obtains the highest NRP (80.8%). As the profile of the NO_x concentration during the lean–rich cycles on the CuO/K_2CO_3/Al_2O_3 catalyst at 400 °C shows, the catalyst exhibits outstanding NSR performance at the beginning, however, with the prolonged operating time, the storage sites can not be fully regenerated and the NO_x removal activity decreases from cycle to cycle. With further increasing the reaction temperature, the NRP of the CuO/K_2CO_3/Al_2O_3 catalyst decreased gradually. At 550 °C, its NRP decreases sharply to 37.5%.

Compared with the CuO/K_2CO_3/Al_2O_3 catalyst, the NSR performance of the CuO/K_2CO_3/$MgAl_2O_4$ catalyst is consistently more effective and steady in the successive 20 cycles in the whole high-temperature region. Additionally, the NRP results show that the NO_x reduction efficiency is poor at 350 °C for both catalysts. It indicates that CuO is only active above 400 °C, which coincides with the NSC results.

3.3. Structure of the catalysts

XRD is employed to investigate the structure of the catalysts. Fig. 4 shows the XRD patterns of the fresh catalysts and the catalysts after NO_x storage at 450 °C. All of the diffraction peaks in Fig. 4a are well matched with spinel-type $MgAl_2O_4$ phase (JCPDS 21-1152). It indicates that the $MgAl_2O_4$ support is successfully synthesized after calcination at 800 °C with no other phase detected. Crystallized CuO phase (JCPDS 48-1548) with 2θ at 35.6°, 38.7° and 48.7° can be clearly identified on the CuO/K_2CO_3/$MgAl_2O_4$ and CuO/K_2CO_3/Al_2O_3 catalysts. No characteristic peak of K-related species is detected on the pattern of the fresh CuO/K_2CO_3/$MgAl_2O_4$ and CuO/K_2CO_3/Al_2O_3 catalysts in Fig. 4b and c, suggesting that the K-related species may be highly dispersed or in amorphous state.[40] Additionally, the mean crystallite size of CuO was calculated on the basis of the XRD data by using Scherrer equation. The mean crystallite size of CuO on the fresh CuO/K_2CO_3/$MgAl_2O_4$ and CuO/K_2CO_3/Al_2O_3 catalysts is 24.4 and 22.4 nm, respectively.

The phase structure of the catalysts after NO_x storage was also characterized as shown in Fig. 4d and e. After the NO_x storage treatment at 450 °C, new diffraction peaks at 27.2°, 29.6° and 32.9° assigned to KNO_3 phase (JCPDS 32-0824) emerge in the XRD patterns of the CuO/K_2CO_3/$MgAl_2O_4$ and CuO/K_2CO_3/Al_2O_3 catalysts. The transformation of carbonates to nitrates is revealed on the K-related storage sites. Stronger peaks of KNO_3

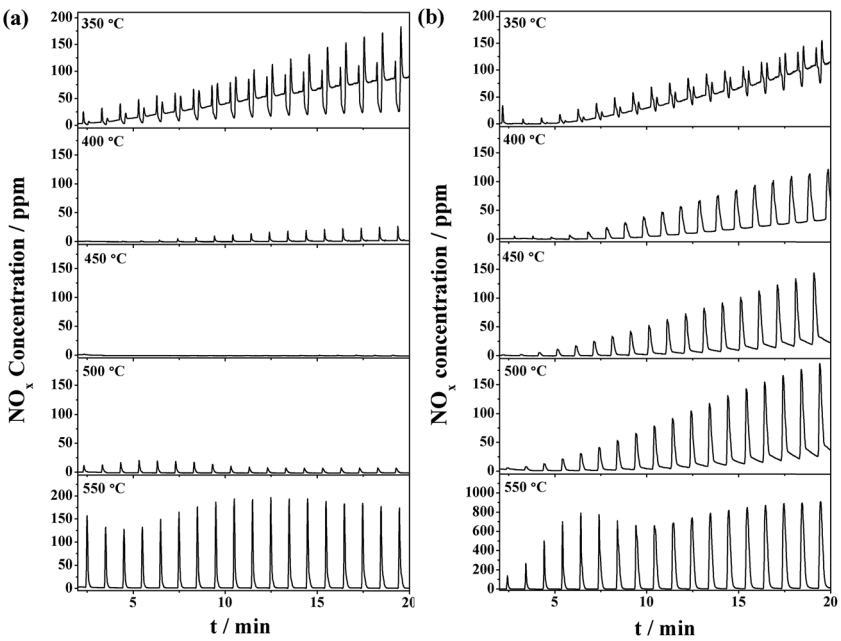

Fig. 3 NO_x concentration curves during the lean/rich cycles over the (a) CuO/K_2CO_3/$MgAl_2O_4$ and (b) CuO/K_2CO_3/Al_2O_3 catalysts.

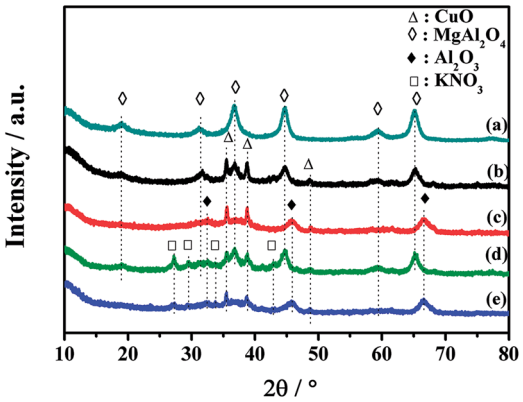

Fig. 4 XRD patterns of the catalysts: (a) fresh $MgAl_2O_4$, (b) fresh $CuO/K_2CO_3/MgAl_2O_4$, (c) fresh $CuO/K_2CO_3/Al_2O_3$, (d) $CuO/K_2CO_3/MgAl_2O_4$ after NO_x storage at 450 °C and (e) $CuO/K_2CO_3/Al_2O_3$ after NO_x storage at 450 °C.

are observed in the XRD pattern of the $CuO/K_2CO_3/MgAl_2O_4$ catalyst than those of the $CuO/K_2CO_3/Al_2O_3$ catalyst, implying that more NO_x was trapped on the $CuO/K_2CO_3/MgAl_2O_4$ catalyst. It is in good agreement with the results of NSC. Additionally, after the NO_x storage, the crystallite size of CuO on the two catalysts is 25.0 and 24.6 nm, respectively, which is similar to the fresh catalysts. Probably, the CuO phase is the active site in the NSR reaction.[29,41]

We measured the specific surface areas of the catalysts by N_2 physisorption. The $MgAl_2O_4$ support has a specific surface area of 100.2 $m^2\ g^{-1}$, lower than the commercial-Al_2O_3 support (179.8 $m^2\ g^{-1}$). After loading the same amount of Cu and K, the surface areas of the $CuO/K_2CO_3/MgAl_2O_4$ and $CuO/K_2CO_3/Al_2O_3$ catalysts drop to 60.5 and 109.8 $m^2\ g^{-1}$, respectively. Combined with the NRP and NSC results, the $CuO/K_2CO_3/MgAl_2O_4$ catalyst owns the higher NSR activity in spite of the smaller specific surface area compared with the $CuO/K_2CO_3/Al_2O_3$ catalyst, suggesting that the specific surface area is not the key factor to determine the catalytic activity of the catalysts.

Fig. S3† shows the SEM image of the fresh $CuO/K_2CO_3/MgAl_2O_4$ catalyst to determine its morphology. The SEM image clearly indicates that the catalyst possesses dense lamellar and needle-like structure, which may be attributed to $MgAl_2O_4$ and K_2CO_3.[42]

3.4. Chemical states of Cu- and K-species

To investigate the chemical states of the Cu- and K-species on the surface of the $CuO/K_2CO_3/MgAl_2O_4$ and $CuO/K_2CO_3/Al_2O_3$ catalysts, the XPS characterization was carried out, as shown in Fig. 5. Fig. 5a displays the XPS spectra in the Cu 2p region of the fresh $CuO/K_2CO_3/MgAl_2O_4$ and $CuO/K_2CO_3/Al_2O_3$ catalysts. For the two catalysts, the Cu 2p spectra are both composed of two typical peaks of Cu^{2+} at about 933.5 eV (Cu $2p_{3/2}$) and 952.9 eV (Cu $2p_{1/2}$) with a satellite shakeup at around 942.3 eV.[43–46] No Cu-related species other than CuO is observed, suggesting the NO_x oxidation and reduction center of the two catalysts is CuO. The above result is in agreement with the XRD result in Fig. 4.

Fig. 5b shows the XPS spectra in the C 1s and K 2p region of the fresh $CuO/K_2CO_3/MgAl_2O_4$ and $CuO/K_2CO_3/Al_2O_3$ catalysts. An apparent peak centering at about 296.1 eV (K $2p_{3/2}$) accompanied by a less intense peak at about 293.0 eV (K $2p_{1/2}$) can be assigned to K^+. Contamination carbon was taken as a reference at 284.6 eV. The C 1s peaks in the region of 278–287 eV are ascribed to the impurities or adventitious in the fresh catalysts.[47] The weak peak locating at 289.7 eV is related to surface carbonate species.[48] In Fig. 5c, the catalysts present a single asymmetric peak of O 1s at about 531.1 eV. It was reported that the C 1s and O 1s peaks of pure K_2CO_3 were at 288.1 eV and 531.1 eV.[47] Therefore, the C 1s at 289.7 eV and O 1s at 531.1 eV may be assigned to K_2CO_3 on the surface of the catalysts.[49] In the preparation process of the catalysts, a part of the K_2CO_3

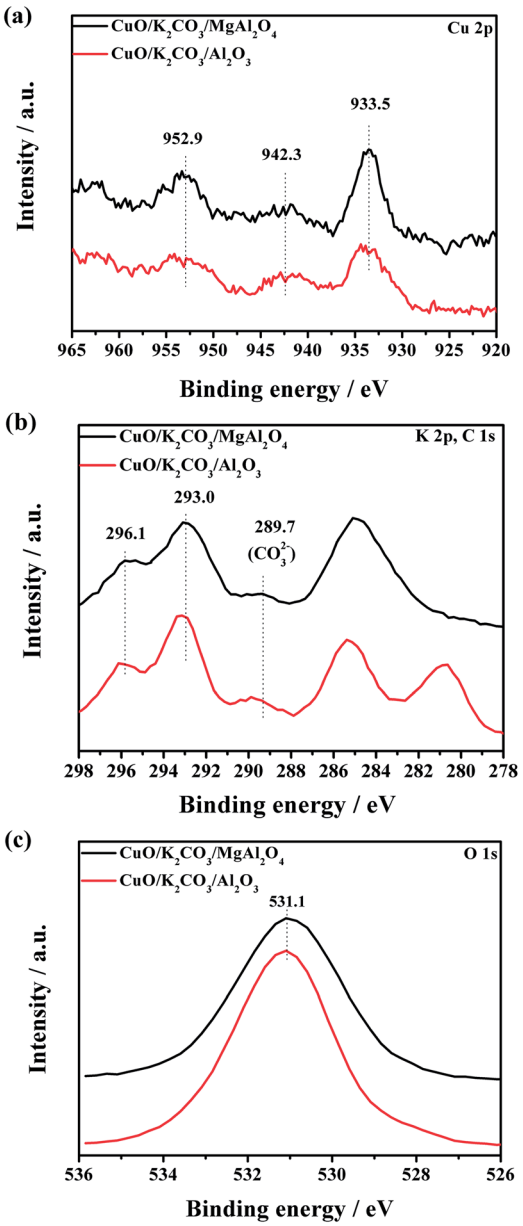

Fig. 5 XPS spectra of the fresh catalysts: (a) Cu 2p, (b) K 2p and C 1s and (c) O 1s.

precursor on the catalysts has decomposed into K_2O and CO_2 during the calcination at 600 °C. However, the K_2O is easy to react with CO_2 and form K_2CO_3 again when the samples are exposed in air. So, the detected K_2CO_3 by the XPS measurement probably results from the reaction of K_2O with CO_2 in air.[50]

The binding energies and elemental compositions from the XPS data are given in Table 2. The surface atomic ratios of Cu/K of the fresh $CuO/K_2CO_3/MgAl_2O_4$ and $CuO/K_2CO_3/Al_2O_3$ catalysts are much lower than their theoretical composition (Cu/K = 0.62). It indicates that the K_2CO_3 may partially cover the CuO phase on the surface of the catalysts. The surface Cu/K atomic ratio of the $CuO/K_2CO_3/MgAl_2O_4$ catalyst is 0.29, larger than that of the $CuO/K_2CO_3/Al_2O_3$ catalyst (0.24). As we discussed in Fig. S1,† the NO_x storage process will be substantially hindered without the aid of CuO. The higher surface Cu/K ratio of the $MgAl_2O_4$-supported catalyst reveals that there is more CuO existing and uncovered on the surface of $CuO/K_2CO_3/MgAl_2O_4$ catalyst, which can improve the accessibility of the active CuO sites, and then enhance the catalytic activity.

To further identify the chemical state of Cu species, Fig. 6 shows the XANES spectra of Cu K-edge of the fresh $CuO/K_2CO_3/MgAl_2O_4$ and $CuO/K_2CO_3/Al_2O_3$ catalysts and the catalysts after NO_x storage at 450 °C. The reference samples are Cu, Cu_2O and CuO. Both of the two fresh catalysts show the similar shape and location of the adsorption edge to that of CuO.[41] There is no Cu and Cu_2O detected on the two catalysts. Therefore, the Cu species on the $CuO/K_2CO_3/MgAl_2O_4$ and $CuO/K_2CO_3/Al_2O_3$ catalysts is in the form of CuO. After NO_x storage, the Cu K-edge of the spent catalysts are also the same as that for the fresh ones, suggesting that little change has taken place for the Cu species before and after reaction. It coincides with the XRD results in Fig. 4. Therefore, CuO is the active component of the $CuO/K_2CO_3/MgAl_2O_4$ and $CuO/K_2CO_3/Al_2O_3$ catalysts.[29,41,51]

The H_2-TPR experiment was conducted to elucidate the reducibility of the fresh catalysts, as shown in Fig. 7. No reduction reaction happens in the profile of the inert $MgAl_2O_4$ support. For contrast, pure CuO shows a H_2 consumption peak at 350 °C. CuO particles on the $MgAl_2O_4$ support and Al_2O_3 support can be reduced at much lower temperature of 240 °C and 238 °C, respectively. After 10% K loading on the CuO/$MgAl_2O_4$ sample, the main reduction peak shifts to 327 °C, which is close to the unsupported-bulk CuO. Notably, a weak reduction peak at 264 °C is observed, which is assignable to the uncovered CuO on the $CuO/K_2CO_3/MgAl_2O_4$ catalyst. While after 10% K loading on the CuO/Al_2O_3 sample, the reduction of CuO occurs at above 300 °C. Herein, only the uncovered CuO on the $CuO/K_2CO_3/MgAl_2O_4$ catalyst can be easy to contact to H_2 and results in the similar reducibility of CuO as the CuO/$MgAl_2O_4$ catalyst. The K_2CO_3 loading on the catalysts may cover the CuO, which can hinder the diffusion of H_2 to CuO. Based on the H_2-TPR result, some of the uncovered CuO by K_2CO_3 exists on the $CuO/K_2CO_3/MgAl_2O_4$ catalyst, while the CuO on the CuO/K_2CO_3/Al_2O_3 catalyst is totally covered. Thus, the $CuO/K_2CO_3/MgAl_2O_4$ catalyst shows a better NSR performance than the $CuO/K_2CO_3/Al_2O_3$ catalyst.

Additionally, the released CO_2 *via* the decomposition of K_2CO_3 during the TPR process can dilute the feed gas and generate pseudo H_2 consumption peaks. The high temperature peaks at 724 °C and 763 °C can be assigned to the decomposition of bulk-like K_2CO_3.

Table 2 Spectra parameters obtained by XPS of the fresh catalysts

Catalysts	Cu $2p_{3/2}$ (eV)	K $2p_{3/2}$ (eV)	O 1s (eV)	Cu/K (atomic%)
$CuO/K_2CO_3/MgAl_2O_4$	933.5	295.9	531.0	0.29
$CuO/K_2CO_3/Al_2O_3$	933.8	296.1	531.1	0.24

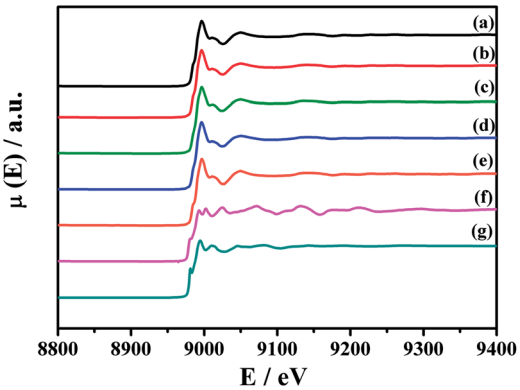

Fig. 6 XANES spectra of Cu K-edge of the samples: (a) fresh $CuO/K_2CO_3/MgAl_2O_4$, (b) $CuO/K_2CO_3/MgAl_2O_4$ after NO_x storage at 450 °C, (c) fresh $CuO/K_2CO_3/Al_2O_3$, (d) $CuO/K_2CO_3/Al_2O_3$ after NO_x storage at 450 °C, (e) CuO, (f) Cu and (g) Cu_2O.

3.5. Property of the supported potassium carbonates on the catalysts

To further investigate the thermal decomposition of K_2CO_3 species, the CO_2-TPD experiments of the fresh $CuO/K_2CO_3/MgAl_2O_4$ and $CuO/K_2CO_3/Al_2O_3$ catalysts were implemented, and the evolution profiles of CO_2 are presented in Fig. 8. As reported in the literature, two kinds of K_2CO_3 with different thermal stability can be distinguished as a function of decomposition temperature.[41] The reaction occurs as the following expression: $K_2CO_3 \rightarrow K_2O + CO_2$. For the $CuO/K_2CO_3/MgAl_2O_4$ catalyst, the desorption of CO_2 at 304–640 °C is regard to the decomposition of unstable surface K_2CO_3 on the catalyst. The second desorption stage within 640–840 °C can be attributed to bulk/bulk-like K_2CO_3 species with the high thermal stability. For the $CuO/K_2CO_3/Al_2O_3$ catalyst, the desorption of CO_2 initiates at 245 °C. The unstable surface K_2CO_3 decomposes from 245 to 763 °C, and the bulk/bulk-like K_2CO_3 decomposes from 763 to 840 °C. By the integration of the CO_2-TPD curves area, we find that the $CuO/K_2CO_3/MgAl_2O_4$ and $CuO/K_2CO_3/Al_2O_3$ catalysts have similar amount of CO_2 desorption, suggesting that the amount of the desorbed K_2CO_3 is similar on the two catalysts. However, the amount of bulk/bulk-like K_2CO_3 on the CuO/$K_2CO_3/MgAl_2O_4$ catalyst is much larger than that on the CuO/K_2CO_3/Al_2O_3 catalyst, suggesting the higher thermal stability of the K_2CO_3 on the $CuO/K_2CO_3/MgAl_2O_4$ catalyst.

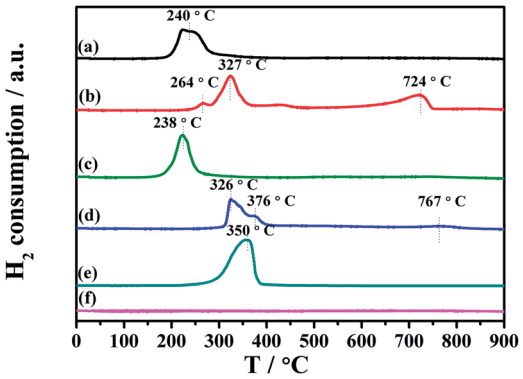

Fig. 7 H_2-TPR profiles of the samples: (a) $CuO/MgAl_2O_4$, (b) $CuO/K_2CO_3/MgAl_2O_4$, (c) CuO/Al_2O_3, (d) $CuO/K_2CO_3/Al_2O_3$, (e) CuO and (f) $MgAl_2O_4$.

In order to explicit the nature of K_2CO_3 species, the FT-IR technique was carried out for the fresh $CuO/K_2CO_3/MgAl_2O_4$ and $CuO/K_2CO_3/Al_2O_3$ catalysts, as well as the references of the bulk K_2CO_3 and $MgAl_2O_4$. Fig. 9 shows their FT-IR spectra. The characteristic peaks of the reference bulk K_2CO_3 appear at 1652 cm^{-1}, 1427 cm^{-1}, 1386 cm^{-1} and 1110 cm^{-1}. The bands at 695 cm^{-1} and 518 cm^{-1} are assignable to typical $MgAl_2O_4$ spinel structure. Compared with the bulk K_2CO_3, the FT-IR spectra of the loaded K_2CO_3 on the fresh $CuO/K_2CO_3/MgAl_2O_4$ and $CuO/K_2CO_3/Al_2O_3$ catalysts shows an additional IR band at 1530 cm^{-1}, belonging to chelating bidentate carbonates.[52] Thus, three kinds of K_2CO_3 species, including bridging bidentate carbonates (1652 cm^{-1}),[53] free ionic carbonate CO_3^{2-} (1410 cm^{-1} and 1110 cm^{-1})[52] and chelating bidentate carbonates (1530 m^{-1}), co-exist on the fresh catalysts.

The IR spectra of the $CuO/K_2CO_3/MgAl_2O_4$ and $CuO/K_2CO_3/Al_2O_3$ catalysts after the NO_x storage reaction at different temperatures were also collected to investigate to the reactivity of the different types of K_2CO_3. Fig. 10a(2–6) shows the IR spectra of the $CuO/K_2CO_3/MgAl_2O_4$ catalyst after the NO_x storage reaction at different temperatures. As reported, both the ionic and bidentate nitrates presented on a series of K_2O/Al_2O_3 catalysts after NO_2 dosing.[54] The most intense peak at 1380 cm^{-1} can be identified as ionic nitrates after the NO_x storage.[52]

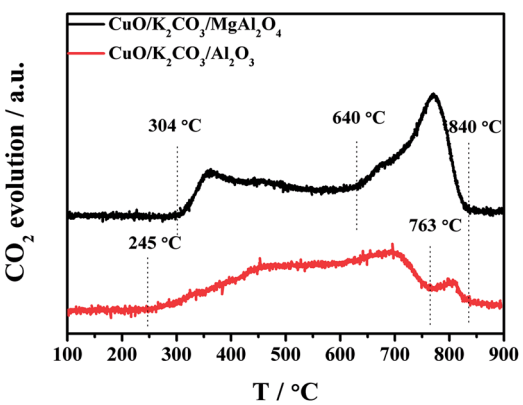

Fig. 8 CO_2-TPD profiles of the fresh catalysts.

The intensity of this peak varies with the reaction temperature of $CuO/K_2CO_3/MgAl_2O_4$ catalyst, the tendency of which is consistent with the NSC order. The intensity of this peak becomes strongest when the $CuO/K_2CO_3/MgAl_2O_4$ catalyst reacts at 450 °C. Differently from the fresh $CuO/K_2CO_3/MgAl_2O_4$ catalyst in Fig. 9, the IR bands of bridging bidentate carbonate and chelating bidentate carbonate almost disappear leaving a tiny amount of carbonate residue on the $CuO/K_2CO_3/MgAl_2O_4$ catalyst, suggesting most of carbonates on the $CuO/K_2CO_3/MgAl_2O_4$ catalyst participate in the NO_x storage. Fig. 10b(2–6) shows the IR spectra of the $CuO/K_2CO_3/Al_2O_3$ catalyst after the NO_x storage reaction at different temperatures. The peak at 1380 cm^{-1} attributed to ionic nitrates can also be detected. However, the peaks at 1652 cm^{-1} and 1530 cm^{-1} do not completely disappear after the NO_x storage process, suggesting that a part of the bridging bidentate carbonate and chelating bidentate carbonate in the $CuO/K_2CO_3/Al_2O_3$ catalyst can not completely store NO_x at high temperatures. Comparing the IR spectra of the $CuO/K_2CO_3/MgAl_2O_4$ and $CuO/K_2CO_3/Al_2O_3$ catalysts after the NO_x storage, there is more K_2CO_3 on $CuO/K_2CO_3/MgAl_2O_4$ transformed to nitrate. It suggests that the $MgAl_2O_4$ can improve the NO_x storage efficiency of K_2CO_3 at high operating temperatures. Additionally, after NO_x storage at 450 °C, the two catalysts were heated in the N_2 flow at 450 °C for 10 min. The IR spectra of the two catalysts after NO_x-TPD are shown in Fig. 10a(7) and b(7). For the $CuO/K_2CO_3/MgAl_2O_4$ catalyst, the intensity of the peak at 1380 cm^{-1} in Fig. 10a(7) has little change compared with Fig. 10a(4). For the $CuO/K_2CO_3/Al_2O_3$ catalyst, a distinct decrease of peak at 1380 cm^{-1} in Fig. 10b(7) is observed compared with Fig. 10b(4). The different behaviors at 1380 cm^{-1} on the two catalysts reveal that the nitrates on the $CuO/K_2CO_3/MgAl_2O_4$ catalyst exhibit higher thermal stability.

3.6. Thermal stability of the stored nitrates

The low thermal stability of the nitrate formed on NSR catalysts in the NO_x storage reaction will limit their application at high operating temperatures.[16] In Fig. 2, the thermal stability of the nitrates on the K sites of the $CuO/K_2CO_3/MgAl_2O_4$ catalyst is

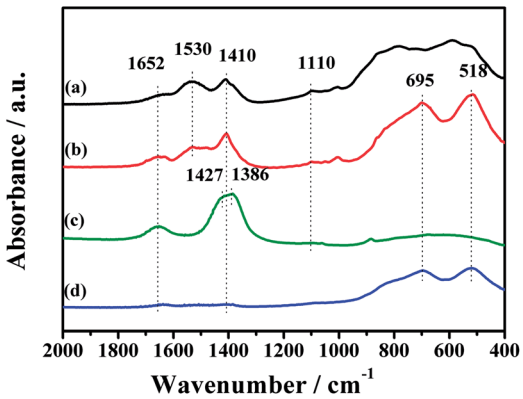

Fig. 9 FT-IR spectra of the samples: (a) $CuO/K_2CO_3/Al_2O_3$, (b) $CuO/K_2CO_3/MgAl_2O_4$, (c) pure K_2CO_3 and (d) $MgAl_2O_4$.

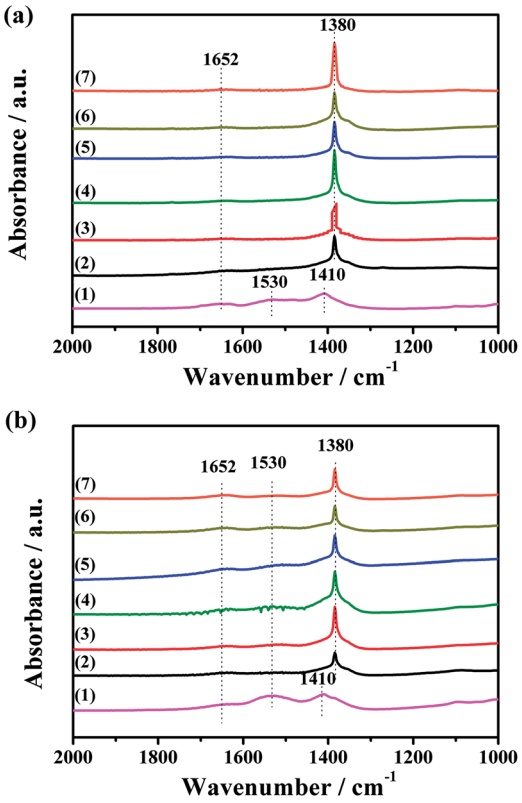

Fig. 10 FT-IR spectra of the (a) $CuO/K_2CO_3/MgAl_2O_4$ and (b) $CuO/K_2CO_3/Al_2O_3$ catalysts: (1) fresh catalyst, and the catalyst after NO_x storage reaction at (2) 350 °C, (3) 400 °C, (4) 450 °C, (5) 500 °C and (6) 550 °C, and (7) the catalyst (4) heated at 450 °C in N_2 flow for 10 min.

higher compared with the $CuO/K_2CO_3/Al_2O_3$ catalyst. Based on the previous report, the strength of N–O bond in nitrate is sensitive to the metal cations exposed from the support because of electronic polarization.[17] The charge density of Al^{3+} and Mg^{2+} is 4.8×10^{-3} e nm^{-3} and 7.5×10^{-4} e nm^{-3}. Lower extent of polarization of Mg^{2+} makes N–O bond less prone to breakage, and thus the nitrates on the $CuO/K_2CO_3/MgAl_2O_4$ show the higher thermal stability.

Additionally, in our study, the temperatures of NO_x desorption correlate to the temperatures of K_2CO_3 decomposition as mentioned in Fig. 8. Thus, the thermal stability of nitrates is related to the thermal stability of K_2CO_3. In other word, the nitrates with high thermal stability may be transformed from the thermal stable K_2CO_3. As discussed in Fig. 10, there is more K_2CO_3 with high thermal stability on the $CuO/K_2CO_3/MgAl_2O_4$ catalyst than that on the $CuO/K_2CO_3/Al_2O_3$, and this part of K_2CO_3 is the main storage sites in the high-temperature NSR reaction. Thus, the trapped nitrate on the $CuO/K_2CO_3/MgAl_2O_4$ catalyst shows the high thermal stability.

Through the above discussion, the $CuO/K_2CO_3/MgAl_2O_4$ catalyst can store much more NO_x than $CuO/K_2CO_3/Al_2O_3$ catalyst above 400 °C, resulting from the former's higher thermal stability of nitrates. The high thermal stability of nitrate is the main reason to induce the high NO_x storage capacity of the $CuO/K_2CO_3/MgAl_2O_4$ catalyst at the high temperatures.

Therefore, with the high thermal stability of nitrates and the high redox capacity of CuO above 400 °C, the $CuO/K_2CO_3/MgAl_2O_4$ catalyst exhibits the prominent NRP performance at high operating temperatures.

4. Conclusion

Herein, we report the high NSR activity of the newly designed $CuO/K_2CO_3/MgAl_2O_4$ catalyst at high operating temperatures. As concerns of the NSR activity in successive 20 lean/rich cycles between 350–550 °C, the $CuO/K_2CO_3/MgAl_2O_4$ catalyst performs more effectively and steadily on De-NO_x in alternative lean/rich atmospheres than the Al_2O_3-supported catalyst. Especially, the NO_x reduction efficiency of the $CuO/K_2CO_3/MgAl_2O_4$ catalyst achieves a maximum value of 99.9% with a large NO_x uptake of 1.56 mmol g^{-1} at 450 °C. Meanwhile, a high N_2 selectivity of 99.7% was also obtained. The NRP of the $CuO/K_2CO_3/MgAl_2O_4$ catalyst maintains above 90% at 400–550 °C. While the NRP of the $CuO/K_2CO_3/Al_2O_3$ catalyst decreases sharply with the increased reaction temperatures.

The states of CuO and K_2CO_3 species have an apparent difference on the $MgAl_2O_4$ and Al_2O_3 supported catalysts. After K loading, CuO is probably covered by K_2CO_3. There is still a part of the uncovered CuO on the $MgAl_2O_4$ supported catalyst, but none for the Al_2O_3 supported catalyst. This part of CuO is beneficial for the oxidation and reduction of NO_x in alterative lean/rich cycles. CuO exhibits the high redox ability at the temperatures above 400 °C. Based on the FT-IR results, the carbonates on the two catalysts can be classified into three types: free ionic carbonate, bridging bidentate carbonate and chelating bidentate carbonate. Most of the K_2CO_3 on the $CuO/K_2CO_3/MgAl_2O_4$ catalyst can convert to nitrates, but only a part of them participates on the $CuO/K_2CO_3/Al_2O_3$ catalyst. Moreover, our results show that the thermal stability of nitrate is consistent with the thermal stability of K_2CO_3. The formed nitrates during the lean operation on the $CuO/K_2CO_3/MgAl_2O_4$ catalyst have the high thermal stability, because of the high thermal stability of K_2CO_3 supported on the catalyst. Accordingly, the $CuO/K_2CO_3/MgAl_2O_4$ catalyst exhibits a high NSR activity at high operating temperatures and is a promising high-temperature NSR catalyst.

Acknowledgements

We are grateful to the National Natural Science Foundation of China [No. 21476159, U1232118], the Program of Introducing Talents of Discipline to China Universities [No. B06006], the 973 program [2014CB932403], and the Natural Science Foundation of Tianjin, PR China [15JCZDJC37400, 15JCYBJC23000]. We gratefully acknowledge Shanghai Synchrotron Radiation Facility (SSRF) for the assistance in the XAFS experiments.

References

1 R. Burch, *Catal. Rev.: Sci. Eng.*, 2004, **46**, 271–334.
2 T. Kreuzer, E. S. Lox, D. Lindner and J. Leyrer, *Catal. Today*, 1996, **29**, 17–27.

3 U. Alkemade and B. Schumann, *Solid State Ionics*, 2006, **177**, 2291–2296.
4 S. Roy and A. Baiker, *Chem. Rev.*, 2009, **109**, 4054–4091.
5 C. H. Kim, G. Qi, K. Dahlberg and W. Li, *Science*, 2010, **327**, 1624–1627.
6 N. Takahashi, H. Shinjoh, T. Iijima, T. Suzuki, K. Yamazaki, K. Yokota, H. Suzuki, N. Miyoshi, S. Matsumoto, T. Tanizawa, T. Tanaka, S. Tateishi and K. Kasahara, *Catal. Today*, 1996, **27**, 63–69.
7 C. Sedlmair, *J. Catal.*, 2003, **214**, 308–316.
8 W. S. Epling, L. E. Campbell, A. Yezerets, N. W. Currier and J. E. Parks, *Catal. Rev.: Sci. Eng.*, 2004, **46**, 163–245.
9 M. Piacentini, M. Maciejewski and A. Baiker, *Appl. Catal., B*, 2005, **59**, 187–195.
10 P. Forzatti, L. Lietti and I. Nova, *Energy Environ. Sci.*, 2008, **1**, 236–247.
11 L. Masdrag, X. Courtois, F. Can and D. Duprez, *Appl. Catal., B*, 2014, **146**, 12–23.
12 B. Pereda-Ayo, J. R. González-Velasco, R. Burch, C. Hardacre and S. Chansai, *J. Catal.*, 2012, **285**, 177–186.
13 J. Dupré, P. Bazin, O. Marie, M. Daturi, X. Jeandel and F. Meunier, *Appl. Catal., B*, 2016, **181**, 534–541.
14 R. D. Clayton, M. P. Harold, V. Balakotaiah and C. Z. Wan, *Appl. Catal., B*, 2009, **90**, 662–676.
15 M. Takeuchi and S. Matsumoto, *Top. Catal.*, 2004, **28**, 151–156.
16 N. Takahashi, S. i. Matsunaga, T. Tanaka, H. Sobukawa and H. Shinjoh, *Appl. Catal., B*, 2007, **77**, 73–78.
17 J. Luo, F. Gao, A. M. Karim, P. Xu, N. D. Browning and C. H. F. Peden, *ACS Catal.*, 2015, **5**, 4680–4689.
18 J. H. Kwak, D. H. Kim, J. Szanyi, S. J. Cho and C. H. F. Peden, *Top. Catal.*, 2012, **55**, 70–77.
19 M. Hatanaka, N. Takahashi, N. Takahashi, T. Tanabe, Y. Nagai, A. Suda and H. Shinjoh, *J. Catal.*, 2009, **266**, 182–190.
20 T. Tanabe, Y. Nagai, K. Dohmae, H. Sobukawa and H. Shinjoh, *J. Catal.*, 2008, **257**, 117–124.
21 L. Lietti, P. Forzatti, I. Nova and E. Tronconi, *J. Catal.*, 2001, **204**, 175–191.
22 S. Roy, N. van Vegten and A. Baiker, *J. Catal.*, 2010, **271**, 125–131.
23 H. Xian, X. Zhang, X. Li, H. Zou, M. Meng, Z. Zou, L. Guo and N. Tsubaki, *Catal. Today*, 2010, **158**, 215–219.
24 W. Wen, X. Wang, S. Jin and R. Wang, *RSC Adv.*, 2016, **6**, 74046–74052.
25 X. G. Li, Y. H. Dong, H. Xian, W. Y. Hernández, M. Meng, H. H. Zou, A. J. Ma, T. Y. Zhang, Z. Jiang, N. Tsubaki and P. Vernoux, *Energy Environ. Sci.*, 2011, **4**, 3351–3354.
26 X. Wang, X. Qi, Z. Chen, L. Jiang, R. Wang and K. Wei, *J. Phys. Chem. C*, 2014, **118**, 13743–13751.
27 R. Vijay, R. J. Hendershot, S. M. Rivera-Jiménez, W. B. Rogers, B. J. Feist, C. M. Snively and J. Lauterbach, *Catal. Commun.*, 2005, **6**, 167–171.
28 Z. S. Zhang, M. Crocker, B. B. Chen, Z. F. Bai, X. K. Wang and C. Shi, *Catal. Today*, 2015, **256**, 115–123.
29 F. Fan, M. Meng and Y. Tian, *Acta Phys.-Chim. Sin.*, 2015, **31**, 1761–1770.
30 T. Tanabe, Y. Nagai, K. Dohmae, H. Sobukawa and H. Shinjoh, *J. Catal.*, 2008, **257**, 117–124.
31 Q. Wang and J. S. Chung, *Appl. Catal., A*, 2009, **358**, 59–64.
32 M. Takeuchi and S. Matsumoto, *Top. Catal.*, 2004, **28**, 151–156.
33 A. J. Ma, S. Z. Wang, C. Liu, H. Xian, Q. Ding, L. Guo, M. Meng, Y. S. Tan, N. Tsubaki, J. Zhang, L. R. Zheng and X. G. Li, *Appl. Catal., B*, 2014, **146**, 24–34.
34 S. Bennici and A. Gervasini, *Appl. Catal., B*, 2006, **62**, 336–344.
35 A. Patel, T. Rufford, V. Rudolph and Z. Zhu, *Catal. Today*, 2010, **166**, 188–193.
36 Q. Wang, J. H. Sohn and J. S. Chung, *Appl. Catal., B*, 2009, **89**, 97–103.
37 J. Despres, M. Elsener, M. Koebel, O. Krocher, B. Schnyder and A. Wokaun, *Appl. Catal., B*, 2004, **50**, 73–82.
38 M. Yung, E. Holmgreen and U. Ozkan, *J. Catal.*, 2007, **247**, 356–367.
39 S. Salasc, M. Skoglundh and E. Fridell, *Appl. Catal., B*, 2002, **36**, 145–160.
40 N. Hou, Y. Zhang and M. Meng, *J. Phys. Chem. C*, 2013, **117**, 4089–4097.
41 Y. Zhang, R. You, D. Liu, C. Liu, X. Li, Y. Tian, Z. Jiang, S. Zhang, Y. Huang, Y. Zha and M. Meng, *Appl. Surf. Sci.*, 2015, **357**, 2260–2276.
42 M. Galvez, S. Ascaso, R. Moliner and M. Lazaro, *Chem. Eng. Sci.*, 2013, **87**, 75–90.
43 J. O. Shim, H. S. Na, A. Jha, W. J. Jang, D. W. Jeong, I. W. Nah, B. H. Jeon and H. S. Roh, *Chem. Eng. J.*, 2016, **306**, 908–915.
44 K. I. Shimizu, H. Maeshima, H. Yoshida, A. Satsuma and T. Hattori, *Phys. Chem. Chem. Phys.*, 2000, **2**, 2435–2439.
45 E. Moretti, M. Lenarda, L. Storaro, A. Talon, T. Montanari, G. Busca, E. Rodríguez-Castellón, A. Jiménez-López, M. Turco, G. Bagnasco and R. Frattini, *Appl. Catal., A*, 2008, **335**, 46–55.
46 F. Márquez, A. E. Palomares, F. Rey and A. Corma, *J. Mater. Chem.*, 2001, **11**, 1675–1680.
47 J. M. Moggia, V. G. Milt, M. A. Ulla and L. M. Cornaglia, *Surf. Interface Anal.*, 2003, **35**, 216–225.
48 X. Deng, A. Verdaguer, T. Herranz, C. Weis, H. Bluhm and M. Salmeron, *Langmuir*, 2008, **24**, 9474–9478.
49 Y. Zhang, M. Meng, F. Dai, T. Ding and R. You, *J. Phys. Chem. C*, 2013, **117**, 23691–23700.
50 Z. Zou, M. Meng and J. He, *Mater. Chem. Phys.*, 2010, **124**, 987–993.
51 X. Wang, Z. Chen, Y. Luo, L. Jiang and R. Wang, *Sci. Rep.*, 2013, **3**, 1559.
52 T. J. Toops, D. B. Smith and W. P. Partridge, *Appl. Catal., B*, 2005, **58**, 245–254.
53 R. You, Y. Zhang, D. Liu, M. Meng, L. Zheng, J. Zhang and T. Hu, *J. Phys. Chem. C*, 2014, **118**, 25403–25420.
54 D. H. Kim, K. Mudiyanselage, J. Szanyi, J. C. Hanson and C. H. F. Peden, *J. Phys. Chem. C*, 2014, **118**, 4189–4197.

